JOURNAL OF MATERIALS SCIENCE 21 (1986) 1093–1110

# Review
# Deformation transitions

A. G. ATKINS
*Engineering Department, University of Reading, Whiteknights, Reading RG6 2AY, UK*
Y.-W. MAI
*Mechanical Engineering Department, University of Sydney, New South Wales 2006, Australia*

All solids with given mechanical properties will fracture brittly when of large enough size; vice versa it is difficult to comminute solids below certain sizes. Both effects are caused by the fracture stress changing with size (according to cube/square scaling principles) whereas the flow stress is essentially independent of size. Again, a fixed size of body, made of different materials, can respond in quite different ways: simple elasticity, elastic fracture, elastoplastic flow, elastoplastic fracture, plastic flow, plastic fracture or plastic collapse are all possible, depending upon the different mechanical properties of the different materials from which it may be made. This review shows that such deformation transitions are controlled by the relative values of size and a material parameter given by $ER/\sigma_y^2$ where $E$ is Young's modulus, $R$ the specific work of fracture and $\sigma_y$ the flow stress. At fixed size of body, made of given material, transitions occur when one or more of the mechanical property terms are altered by rate, temperature, environment, superimposed hydrostatic stress and so on. A wide range of examples is used to illustrate these effects, and their role in load-bounding methods in elastoplastic design of structures is considered.

## 1. Perceived wisdom on fracture and transitions

Common experience tells us that under similar conditions of loading, different materials deform and break in different ways. At the one extreme ice, glass, blackboard chalk, bone, cello-strings, rubber bands and the like break suddenly without warning; and some materials will shatter into many pieces. At the other extreme soft metal wires, lead sheet, pitch, chewing gum, polyethylene film, and so on, first experience plastic yielding or visco-elastic flow, which produces extensive deformation before eventual fracture – and sometimes fracture is difficult to achieve in materials such as modelling clay. In between these extremes are materials such as some cold-worked metals and several rubber-modified polymers which, under similar conditions of loading, suffer a limited amount of permanent deformation before fracture.

On the basis of this common experience, it is customary to classify the behaviour of materials at room temperature broadly into two types of fracture, namely brittle and ductile, the distinguishing feature between which is whether the broken parts may be refitted together to regain essentially the original dimensions. Archaeologists can reconstruct ancient vases from pottery shards because the fracture was brittle, but it is impossible to refit together the portions of an opened beer or sardine can unless the wound-up bit is plastically uncurled.

When conditions change, the same size piece of material may behave differently, depending on how the relative resistance to fracture and flow change. For example, increase in temperature usually softens materials, so that flow takes over from fracture (consider the well-known brittle–ductile transitions in Charpy tests on b c c and some h c p metals; the manufacture of glass bottles and the drawing of glass fibres at high temperatures compared with the brittle behaviour of glass at room temperature – or the extensive hot-stamping industry based on the hot ductility of $\beta$-brasses which at room temperature are comparatively brittle). Increase of temperature which removes moisture, on the other hand, promotes brittleness (consider wet and dry mud, wet and dry wood). Increases in the rate of deformation usually promote brittle behaviour in a given material (consider pitch which flows at low stresses over long periods of time, but which may be snapped brittly when stressed in short times, and also "silly putty"). Changes in environment may promote either brittleness (consider hydrogen embrittlement in steels and liquid-metal embrittlement in steels and aluminium) or flow (consider the Joffé effect [1]) and a given material may be affected in different ways by different environments (high impact polystyrene is made brittle by sunlight, but its threshold resistance to fatigue cracking is increased by soaking in alcohols).

Changes in microstructure of materials with similar compositions can also be important. In metals, for example, coarse-grained zinc is brittle at room temperature whereas fine-grained zinc can be deformed to 90% reduction of area in a tensile test. This comes about because small grains produce small glide bands and hence slip-induced microcracks of short length in

0022–2461/86 $03.00 + .12 

comparison with those produced in large grains; as explained later, shorter cracks require higher stresses to cause fracture, and in the case of zinc of adequately small grain size, since the fracture stress in a laboratory tensile specimen exceeds the yield stress, flow will precede fracture. High-temperature creep-resisting alloys, which typically possess large grain diameters so as to avoid a lot of grain-boundary sliding, are not particularly tough at room temperature unless special alloying additions are used. The effects of ageing and irradiation on metallic microstructure cause embrittlement.

Some alloying elements tend to promote ductile behaviour, either because of their effect on gross microstructural features, or their effect on the metallic lattice. For those microstructural variables that are well understood in crystalline solids, the one common factor in increasing ductility appears to be the suppresion of void formation and growth of microcracks. The "cleanliness" of the microstructure of commercial alloys (inclusion content and its geometric distribution and shape) is vital in this context. For example, less than 0.01% bismuth has a potent effect on the ductility of copper, and the effect of the geometric shape and distribution of second phases on ductility is strikingly displayed between flake and spheroidal cast irons. Manganese is a desirable alloying element in steels containing sulphur since MnS inclusions are relatively harmless, unlike FeS which encourages grain-boundary brittleness.

Fracture in "damage-free" glass (i.e. glass in which best attempts have been made to remove the surface microcracks from which normal fractures start) is also affected by micro-inclusions. For example, NiS changes its crystal structure at 300° C giving an increase in volume, so that some glass failures have been attributed to residual stresses around NiS inclusions. (Heavy metal sulphides are among the few minerals insoluble in soda-lime glass and not wetted by it.)

A major factor controlling the occurrence of fracture or flow is the state of stress, an indicator of which is the hydrostatic or mean stress $\sigma_H = (\sigma_1 + \sigma_2 + \sigma_3)/3$ where $\sigma_1$ etc., are principal stresses. It is well-known that compressive $\sigma_H$ encourages plastic flow rather than brittle fractures in rocks (von Kaŕmán) and zinc (Böker) (see Nadai [2]) which may explain the tortuous flow of otherwise brittle rocks in the Earth's crust. "Brittle" metals may be plastically formed successfully by means of hydrostatic extrusion where the billet is surrounded by fluid under high pressure in the container, and extruded into fluids which themselves are under pressure. The effect of residual or manufacturing stresses can also be thought of in terms of the sign and magnitude of $\sigma_H$. Residual tensile stresses significantly affect stress-corrosion cracking, and residual compressive stresses deliberately introduced into the surface of machine parts (by, for example, shot-peening) inhibit fatigue crack initiation and propagation.

Hydrostatic compression exists under many indenter geometries so, owing to its suppressive effect on crack formation, plastic flow can often be produced in hardness tests on materials which would fracture brittly in tension. Added to that, change in indenter shape can itself produce transitions in deformation. The role of indenter geometry is highlighted when sideways tractions are introduced as in abrasive machining. It is found that the cross-sectional area of the groove formed as an abrasive particle slides on the surface of a ductile metal shows a transition with orientation and geometry of the scratching tool.

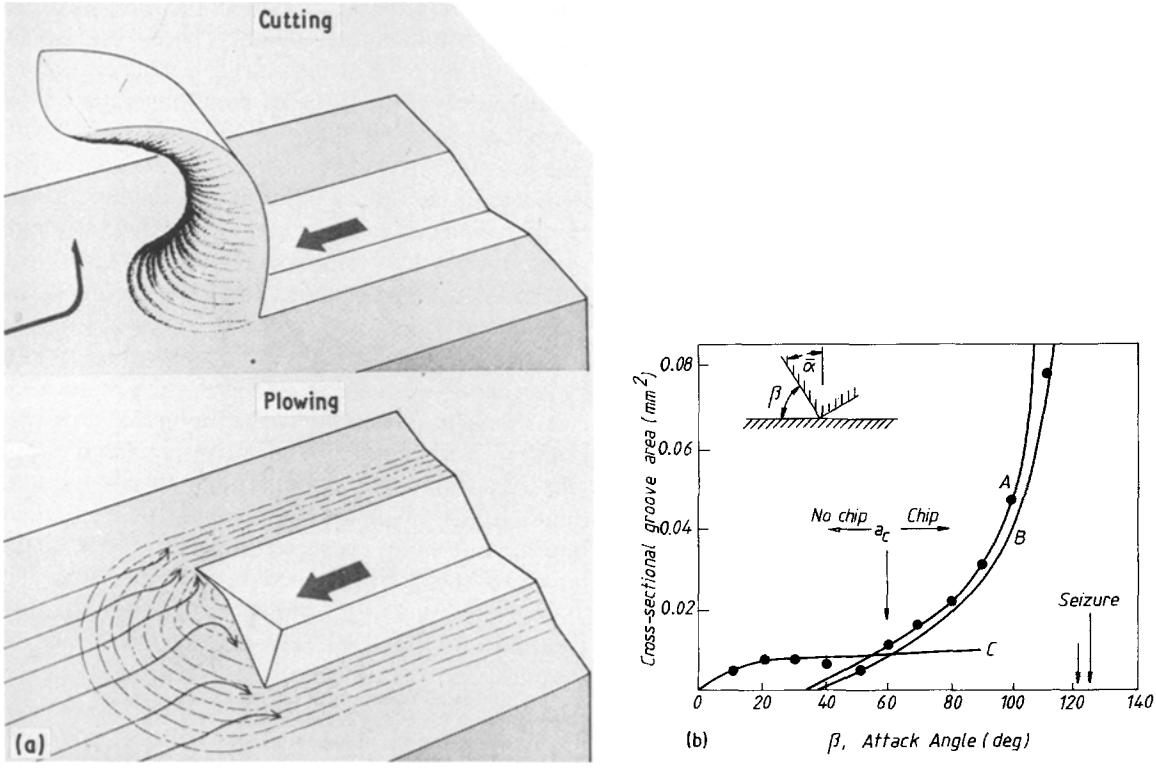


*Figure 1* (a) Cutting and ploughing observed in abrasive machining (reproduced from Samuels [3], with permission) and (b) transition between chipping and no chipping in abrasive machining (after Sedricks and Mulhearn [4]).

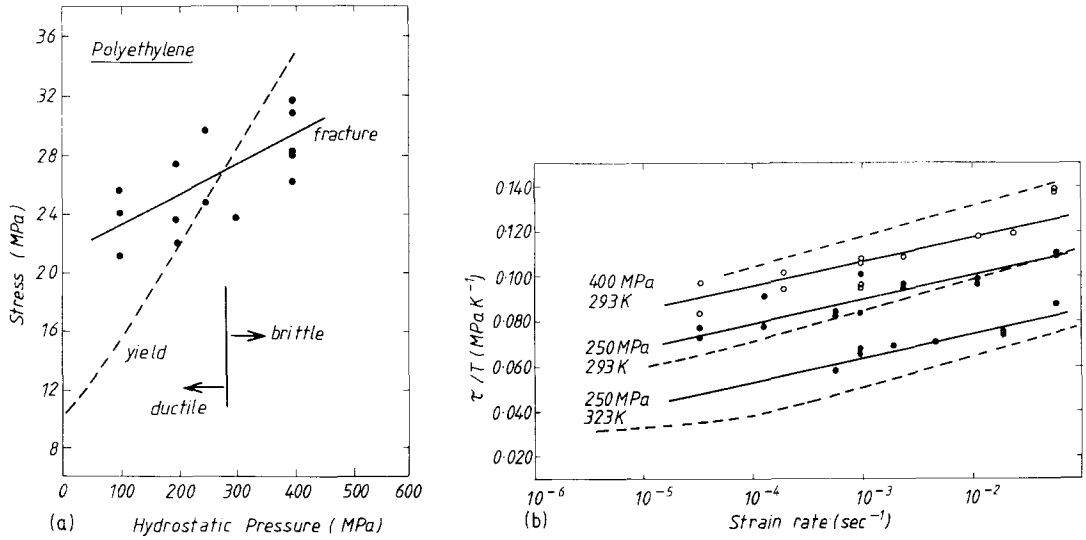


*Figure 2* (a) Fracture stress as a function of pressure for notched samples of Rigidex 50 tested in Igepal solution at 293 K and a strain rate of $9.4 \times 10^{-4}$ sec$^{-1}$ and (b) fracture and yield stresses as a function of strain rate, temperature and pressure for Rigidex 50 tested in Igepal solution (both reproduced from Truss *et al.* [6] with permission).

For given frictional conditions and load, there is a critical "attack angle" for the tool below which a chip or ribbon fails to be cut; instead a prow of material is formed ahead of the tool which is moved into side ridges alongside the groove as the tool "rubs along" (Fig. 1a). The attack angle, $\beta$, is measured from the horizontal and corresponds with $\beta = (90 + \bar{\alpha})$ where $\bar{\alpha}$ is the tool rake angle as conventionally defined from the vertical. The critical attack angles for a range of metals being scratched with pyramidal tools are roughly as follows: copper, 45°; α-brass 55°; lead, 60°; nickel, 70°; aluminium, 85°. At larger attack angles, when ribbons of material are machined away, the size of groove increases rapidly and eventually seizure occurs as the tool "digs-in" (Fig. 1b). Other things being equal, ribbons are formed when scratching with pointed indenters in facet-first orientation, but in edge-first orientation a piled-up groove is produced [5]. There is another type of transition in this sort of situation which concerns whether a ribbon is cut or whether fragmentation of the workpiece in the track of the tool occurs (i.e. "lumps are knocked out").

Polyethylene usually behaves in a ductile fashion, but Ward and co-workers (e.g. [6]) have shown that the pressure dependence of the fracture stress of "Rigidex 50" (a high-density homopolymer manufactured by BP Chemicals Ltd,) is significantly lower than the pressure dependence of its yield stress. Thus with the application of sufficiently high hydrostatic pressure, the yield stress may be made higher than the fracture stress and brittle behaviour results (Fig. 2a). Again in this material, transitions can be produced by changing the *strain-rate*, since the strain-rate dependence of the fracture is less than that of the yield stress (particularly at high strain rates, high pressures or low temperatures, Fig. 2b). Similar behaviour is known in poly(methylmethacrylate) (PMMA) and polycarbonate (PC) [7, 8], and parallels those studies in which strain-to-fracture has been noted to decrease with increasing pressure [9, 10]. It should be noted that in some of Ward *et al.*'s experiments, brittle failure of polyethylene could only be induced by notching the samples and subjecting them to an agressive environment under pressure (the Igepal solution mentioned in the caption to Figs. 2a and b is the environment recommended by the American Society for Testing and Materials (ASTM) for standard tests on the susceptibility of polyethylenes to environmental stress cracking). It would appear, therefore, that one effect of hydrostatic pressure is to reduce the time scale within which environmental stress cracking is observed.

The most well-known, and perhaps most studied, deformation transition concerns changes in Charpy or Izod impact energy of steels with temperature. Over similar narrow temperature ranges, marked changes also occur in % reduction of area and % elongation in other bcc and some hcp metals and some polymers [11]. Fig. 3a shows how change of temperature produces transition in another type of test; namely, when balls of various sizes are indented to a depth of one radius in blocks of PMMA. The percentage of uncracked indentations is plotted against temperature. Fig. 3b shows similar transitions produced by environmental effects. The critical radius at which at least one radial fracture was observed changes with solvent solubility parameter $\delta_s$ when the surface being indented is flooded with solvent.

A different environmentally induced transition is the steaming of wood in order to bend it without splitting. Water has a powerful influence on the properties of biological materials: a soggy biscuit is an example of a deformation transition from the crisp dry state, and loss of turgor pressure in plants causes them to wilt and become flaccid.

Notches encourage brittle fracture owing to increased tensile $\sigma_H$ near the root of the notch; thus Charpy and Izod notched impact tests arguably measure the resistance to fracture under high tensile $\sigma_H$, as well as some high strain-rate "impact strength". In thick structural sections, the constraint of the surrounding material promotes high tensile mean

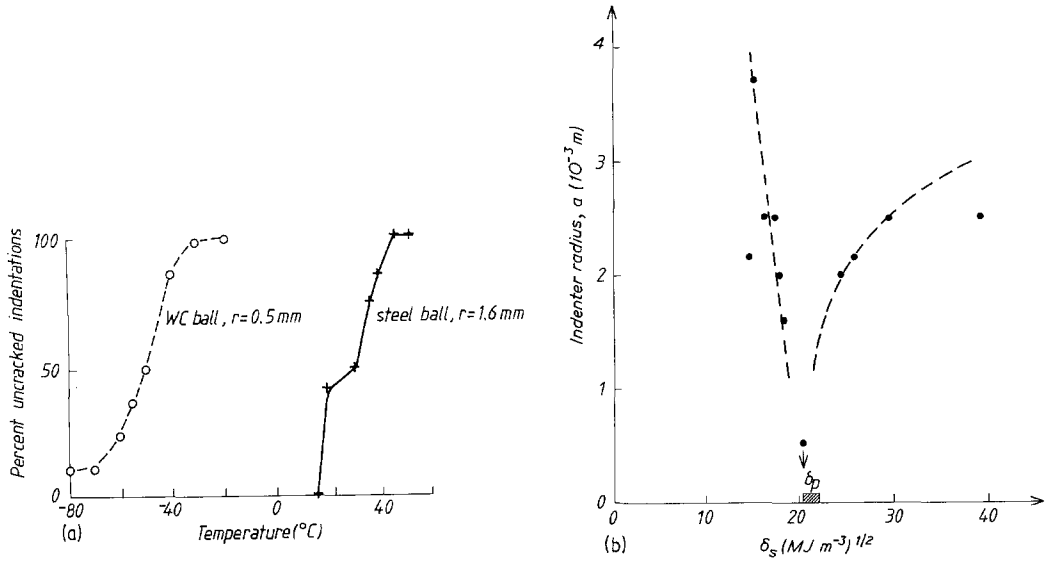


*Figure 3* (a) Upper transitions between elastoplastic flow and elastoplastic fracture caused by change of temperature in identation tests on PMMA. ○ WC balls of radius 0.5 mm and steel ball of radius 1.6 mm (Puttick *et al.* [51]. (b) Critical radius of the indentation plastic zone separating flow and fracture beneath a ball in PMMA as a function of solubility parameter of liquid environment (courtesy M. Omar).

stresses in the internal centre regions of the body which thereby have a lower resistance to fracture than thin pieces of the same material. A different, but related, method of changing constraint is exhibited when sandwiches of brittle and ductile components are made. It is possible to suppress yielding and produce brittle fracture in ductile materials in this way (Fig. 4) and, knowing the appropriate mechanics to apply, is a useful method for the determination of elastic fracture properties in laboratory-sized testpieces.

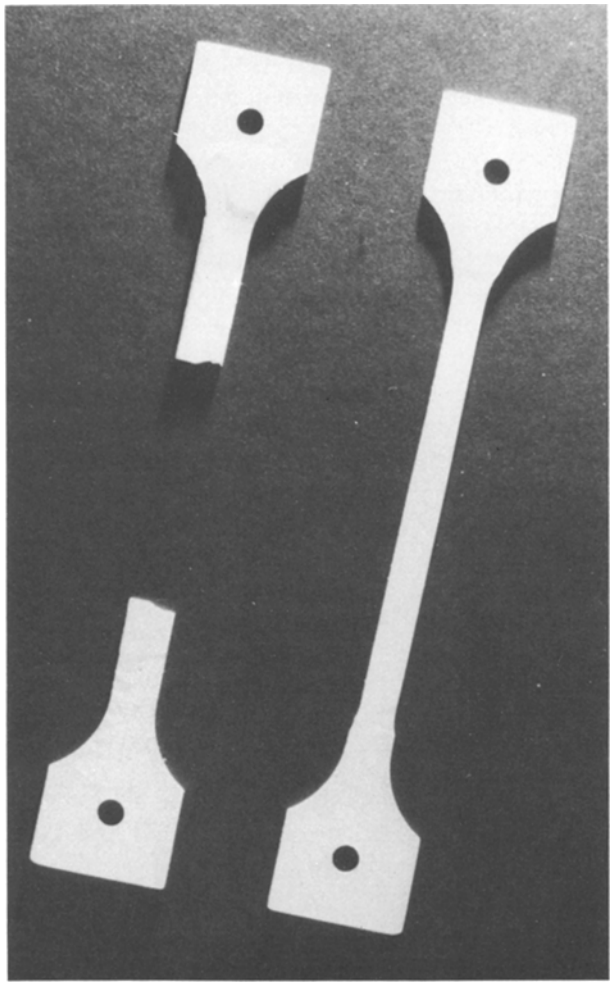

*Figure 4* Tensile testpieces of polyethylene, the left coated with epoxy, the right uncoated. The coated specimen broke brittly, the natural specimen flowed plastically and drew down (courtesy R. Dakin).

Transitions with change of size are familiar in fracture toughness testing where there are limitations on the minimum sizes of testpieces in order to inhibit yielding. A transition between elastic and elastoplastic fracture is found in a quality control test for spot welds. A cruciform testpiece formed by spot welding two strips is pulled apart normal to the sheet thickness and depending on the relative size of weld diameter and sheet thickness, failure occurs either by cracking across the weld junction at lower loads or by pulling out a plug of (ductile) metal in shear at higher loads. Interfacial fracture occurs at small weld diameter-to-sheet thickness ($d/B$) ratios, and vice versa for plug formation (Fig. 5). In a similar vein, Kendall [12] has demonstrated the impossibility of comminuting small particles by compression since, when the deformation zone is small enough, even the most brittle solid will flow.

Our consideration of transitions has been qualitative so far. But is it possible to be quantitative and describe events in terms of material and geometric parameters? When some people say that glass "cannot" be turned in a lathe because it is too "brittle", what is meant by that? Why in the machining of steel do we not see the sort of brittle "splitting" displayed in the fracture of large structures made from the same material; why, indeed, do we find respectable % reductions in area when small testpieces are taken from such large structures? What thickness of a ductile polymer needs to be embrittled by ultraviolet radiation so that the sandwich as a whole will snap and not flow? And so on.

The following sections explore the mechanics of deformation transitions. Not only do we attempt to identify the conditions at the boundaries of the transitions between modes of deformation, but we also investigate whether there is a progressive change in "degree of deformation" within one mode. That is,

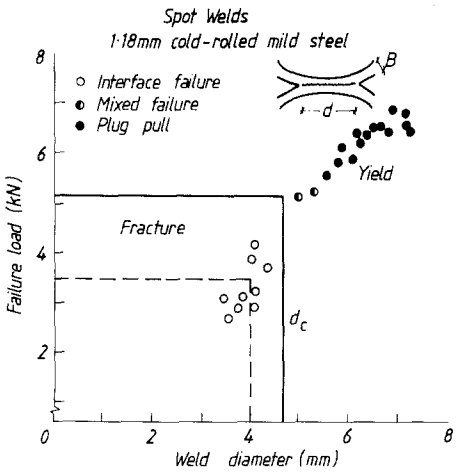


*Figure 5* Fracture transitions in spot weld cruciform tests (after Smith [48]).

when fracture is preceded by extensive flow because the size of specimens is too small to permit elastic fracture from the outset, for example, in what way does the amount of plastic flow before fracture depend on the size of the cracked body?

Again, although most discussion in this review relates to monotonic loading, size effects within one mode of deformation are well-documented in high cycle fatigue (see, for example, Heywood [13]). The applied stress (however defined) required to fracture a specimen depends on its size, so that the absolute level of stress at a given lifetime, or the life at constant stress, are functions of some linear dimension. This statement applies particularly to inhomogenous stress fields as in the bending of plain test pieces or any loading of notched bars. Until recently, these effects have not had adequate explanation (statistical arguments regarding the distribution of flaw sizes in common ductile engineering metals are not convincing) and the role of crack propagation rates to total fatigue life and/or strength has now been investigated [14].

Some elementary mechanics behind changes in fracture stress with size, in both monotonic and fatigue loading, are explored in the next section. If fracture stresses change with size, circumstances arise in which changes in mode of deformation can occur. An understanding of these mechanics will help us in a quantitative assessment of that particular cause of deformation transition: consideration of quantitative assessment of transitions caused by other effects (temperature, rate, constraint to flow, environment, etc.) follows after that.

## 2. Scale effects

### 2.1. Monotonic elastic fracture

Ludwik in 1909 [15] described the role of changing stress states in terms of raising or lowering the stress–strain curve relative to a "fracture stress" curve characteristic of the material, as shown schematically in Fig. 6a. Increase of strain rate, increase of $\sigma_H$ (notches and/or thick sections), or decrease of temperature tend to raise the $\sigma$–$\varepsilon$ curve as shown thus giving smaller strains to fracture (points A . . . D where the $\sigma$–$\varepsilon$ curve intersects the fracture curve). *Notch-brittleness* may be explained if the characteristic fracture stress, $\sigma_f$, is approximately constant with temperature (Fig. 6b) and the variations of uniaxial yield stress ($\sigma_y$) and fully constrained uniaxial yield stress

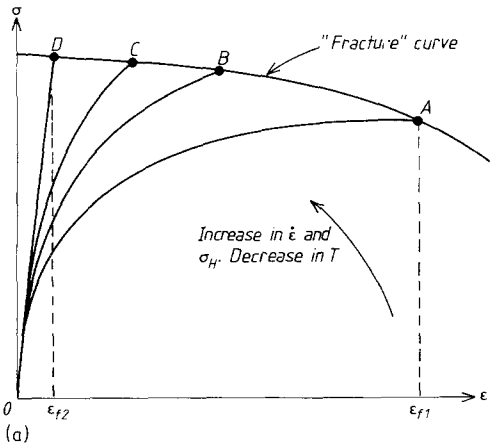


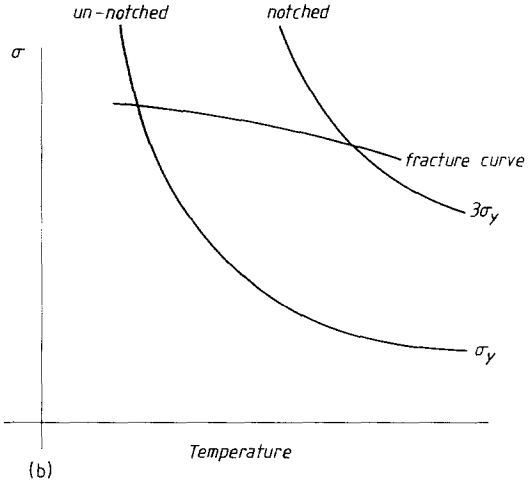


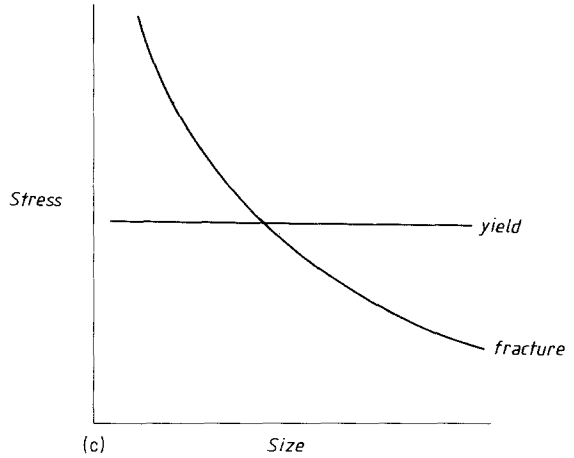


*Figure 6* (a) Ludwik's early idea of a "fracture stress" curve which was supposed to be a material property, (b) Orowan's classification (based upon a material-property fracture stress curve) of solids into "simply brittle," "notch-brittle" and "simply ductile," (c) size (or scale) effect in the mechanics of fracture. The stress to cause cracking often falls with increase in size of the cracked body (it depends on the geometry, scaling and method of loading and is the result of cube/square scaling). The stress to cause plastic flow, on the other hand, is usually considered to be independent of size. Hence large structures, made of materials which behave in a ductile fashion in the laboratory, can fracture in a brittle fashion if they are large enough. Vice-versa it is difficult to comminute powders below certain sizes, owing to flow supervening fracture in small sizes.

($3\sigma_y$ in the presence of deep notches) are plotted on the same diagram. Materials are simply ductile at high temperatures where $\sigma_f > 3\sigma_y$; at low temperatures where $\sigma_f < \sigma_y$ the material is simply brittle; when $\sigma_f < 3\sigma_y$, Orowan [16] called the material notch-brittle, i.e. ductile in plain tensile tests but brittle in notched tests having large plastic constraint. As shown later, the idea of a single "fracture stress curve", which is representative of the material is *not* correct and although Figs. 6a and b are useful conceptually, they are wrong in general.

It is not always appreciated that in the mechanics of fracture, unlike the mechanics of plastic flow, there is a *scale effect* whereby the stress to cause fracture in a large body may be smaller than the stress to cause fracture in a similar, but smaller, body. This follows from the basic formulae for cracking stresses of the sort: $K_c^2 = ER = \sigma_f^2(\pi a)Y^2$, where $K_c$ is the critical stress intensity factor, $E$ is Young's modulus, $R$ the specific work of fracture, $\sigma_f$ the fracture stress, $a$ the flaw size, and $Y$ the shape factor for the particular cracked geometry in question. For two geometrically similar bodies with identical microstructures and mechanical properties, $\sigma_f a^{1/2} = \sigma_f(a/D)^{1/2}D^{1/2}$, where $D$ is size, is constant at fracture, so [17–19]

$$\sigma_{f(large)} = \sigma_{f(small)}/\lambda^{1/2} \quad (1)$$

where $\lambda$ is the scaling factor. Of course, not all "prototype" structures and components are geometrically similar versions of laboratory "models": it is possible to test ship's plate in full thickness in the laboratory but impossible to duplicate the extent of the hull; annular sections of pipelines may be tested in the laboratory but there is a limit to the length, and so on. The scaling laws for non-proportionately scaled elastic structures have been derived [20] where there are four separate scaling factors for height, width, thickness and crack length. The details need not concern us here but we note that, usually, fracture stresses in the prototype are smaller than fracture stresses in the model. The physics behind this conclusion relates to cube/square scaling: the energy available to feed the crack goes up as the volume increases but the energy required for fracture increases only as crack area increases. Puttick [21] has drawn the analogy with critical sizes of nuclei in thermodynamic nucleation theory, and cube/square scaling enabled Brunel to design the "Great Western" large enough to cross the Atlantic and have coal to spare.

The consequence of the scale effect in elastic fracture is that in large bodies the fracture stress may be brought down below the safety-factored yield stress on which traditional strength-of-materials design is based and the structure will unexpectedly break in a brittle fashion even though small samples taken from the same body will be ductile in the laboratory. Fig. 6c illustrates this effect. There is thus a mechanics explanation for the "brittle fracture story" which applies irrespective of any changes in micromode of fracture. Indeed it is true to say that the fracture of Vierendeel bridges, welded ships and so on (which gave birth to the modern discipline of fracture mechanics) could have been explained at the time in terms of the Griffith theory [22, 23]. What was not understood was that Griffith's analysis and experiments on glass could be applied to *all* globally elastic fractures, i.e. fractures in which all irreversibilities are in a boundary layer contiguous with the crack faces. Such fractures are (at least in engineering terms) "reversible" and, of course, a number of ships were repaired by welding them back up.

Irwin in 1954 [24] recognized that explanations of size effects prior to that time neglected the influences of elastic energy in the cracked bodies: he remarked that,

". . . disregarding size effects due to changes in materials properties with size caused by problems of metallurgical processing, previous studies have shown that fracture size effects of significant magnitude exist in solids whether they are brittle or ductile and whether the material is a metal or a plastic. The most elaborate precautions to eliminate differences due to material quality, lack of precise similarity of dimensional ratios, specimen surface preparation, and the experimental loading devices have failed to remove fracture size effects. It is apparent that these are fundamental to the nature of the severing process. . . ."

The particular symposium, at which he spoke, was concerned with low-temperature effects but he cautioned that reduced ductility with temperature was not the sole reason for brittle fracture in large structures, and thereby undermined the usual "metallurgical" explanation for this sort of thing. Of course, if the resistance to fracture does fall for some reason, fracture stresses will be diminished even more. But it is important to be aware that even without such changes in toughness, brittle fracture can occur in large bodies made of materials behaving ductilely in the laboratory.

## 2.2. Elastoplastic fracture

Early reports [25–27] of experiments on geometrically similar notched three-point bend bars of ductile metals demonstrated that (i) the extent of plastic flow before cracking is smaller in larger testpieces, and (ii) the relative amount of total work done after peak load is smaller in larger testpieces. Figs. 7a and b show similar results taken from Shearin *et al.* [28] for three-point bending and Hagiawara *et al.* [29] for notched and un-notched scaled I-beams. Clearly, larger testpieces fracture earlier than smaller, which accords with general ideas on size-effects described in Section 2.1, namely that bodies which are "large enough" may fracture in a brittle (globally elastic) fashion, even though small bodies of the same material may undergo extensive plastic flow before fracture. Also, as shown in this figure, no bodies fail in a truly elastic fashion (i.e. in the early linear reversible portion of the curves), but we make the important observation that there is a continuing scale-effect within the elastoplastic fracture range, and that larger bodies undergo less elastoplastic flow before final fracture than scaled smaller bodies.

It is clear from Figs. 7a and b that until the final load drop, data from all sizes of cracked body follow the

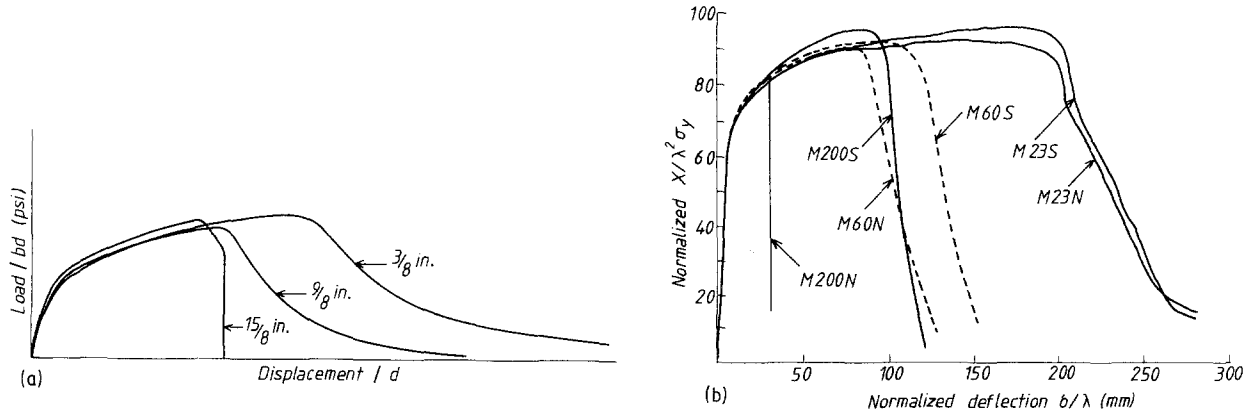


*Figure 7* (a) Elastoplastic fracture of geometrically similar 3-point bend testpieces of low carbon steel (Shearin *et al.* [28]) and (b) elastoplastic fracture of geometrically similar notched and un-notched I-beams (Hagiawara *et al.* [29]).

same master curve. The master curve is the effective stress–effective strain, $\bar{\sigma}-\bar{\varepsilon}$, curve for elastoplastic flow for the material. That all the results follow the same master curve (within the limits of experimental measurement and material reproducibility) is another way of saying that there is no scale-effect in simple plastic flow.

It is explained in Shearin *et al.* [28] that cracks begin to grow *before* the final drop in load. Consequently, the different normalized displacements at final fracture in specimens of different sizes are connected with crack *instabilities* in elastoplastic fracture in those different testpieces rather than crack *initiation*. Indeed, application of a critical $J$-integral value, $J_c$, or critical plastic work/volume criterion of crack initiation in a rigid-plastic body would predict approximately the same normalized displacement at fracture, independent of size, since the area under a $\bar{\sigma}-\bar{\varepsilon}$ curve is the plastic work/volume. Elastoplastic crack instabilities are not within the scope of this review and the interested reader is referred to Atkins and Mai [19]. The field (particularly with regard to quantitative assessment) is comparatively unexplored and is the subject of current research. For present purposes we note that inspection of crack growth resistance ($J_R$)-based finite element procedures for elastoplastic crack instabilities seems to indicate a size effect along the lines indicated in Figs. 7a and b, although size effects *per se* were not being looked for in that work.

### 2.3. Fatigue fracture

It has recently been pointed out that any fatigue crack growth law which incorporates the stress intensity factor (such as the Paris power law equation for Stage II growth) must exhibit a scale effect [14, 19]. In geometrically similar bodies, for example, it may be shown that crack growth rates, $da/dN$, are faster in the larger body at the same relative position in the path of fracture (same $a/D$ where $D$ is the width of the body). What effect that has on the number of cycles to failure as between large and small bodies depends on the starting and final flaw sizes. That is, $(da/dN)_{large} > (da/dN)_{small}$ but cycles to fracture depend on the distance the crack has to run. Of course, fatigue lives of plain samples relate to initiation as well as propagation and the initiation phase can take up the major portion of fatigue life in high cycle fatigue. Consequently scaling laws derived from Paris-type growth laws can tell only part of the story. In the case of welds, however, the analyses are likely to be directly applicable since the inherent tiny intrusion defects associated with welds act as initiation regions for Stage II propagation to occur directly. It is of note that Burdekin's finite element calculations for fatigue of fillet-welded joints [31] show (i) that for a given attachment thickness and weld size, increasing the main plate thickness gives an increasing tolerance for initial defects, but (ii) that when the attachment thickness and weld size are scaled up in proportion to the main plate thickness, increase in the size of the joint leads to a dramatic drop in tolerance for initial defects at larger thickness. Calculations can be performed for Paris-law fatigue growth in non-proportionately scaled bodies [19].

## 3. Flow or fracture?

Is it possible to say beforehand how a given solid, of given geometry subjected to given applied loads, will deform? As far as time-independent deformation is concerned, two pairs of questions have to be answered:

1. Is the strain state elastic or plastic?
2. Is it favourable for cracks to initiate and propagate or not?

The first equation is easily answered by the magnitude of the strains induced by the applied loads, $\varepsilon_a$. If they are greater than the yield strain, $\varepsilon_y$, then clearly the body has become plastic. Calculations are straightforward if the deformation is uniform (e.g. uniaxial tension of an homogeneous isotropic bar, and also multiaxial uniform loading using effective stresses and strains and the plasticity yield function). For non-uniform loading, $\varepsilon_a$ will be non-uniform and there may be mixed regions of elastic fields ($\varepsilon_a < \varepsilon_y$), elastoplastic fields ($\varepsilon_a \approx \varepsilon_y$) or fully plastic fields ($\varepsilon_a \gg \varepsilon_y$).

The answer to the second question is more difficult to tackle and should be sub-divided really depending upon whether or not there are pre-existing cracks in the body (which of course will produce non-uniform deformation fields and affect the answer to question 1). It is helpful to consider the ratio of the specific work *required* for cracking, $W_r$, to the energy rate, $W_a$, in the

loaded body which may be *released* for cracking. In elastic fracture in a body already containing a sharp crack, $W_r$ is identified with the material fracture toughness $R$; under the same circumstances $W_a$ is $-(\partial\Lambda/\partial A)_u = J$ or $G$ the potential energy release rate, and $W_r/W_a = R/G$ in a linear system. In plastic fracture of metals, $W$ is the specific essential work of initiation, $J_i$, given by $-(\partial U_T/\partial A)_u$, where $U_T$ is the total work area beneath a load–displacement plot, or by related expressions, and which is linked to microstructures [19]. In this case, $W_a$ is the history-dependent $\int(\sigma_H/\bar{\sigma})d\bar{\varepsilon}$ or some version of it, or related quantities such as the crack opening displacement [19]. Thus,

1. when $\varepsilon_a < \varepsilon_y$ and $W_r > W_a$ we have simple elastic deformation;
2. when $\varepsilon_a < \varepsilon_y$ and $W_r < W_a$ we have elastic brittle fracture;
3. when $\varepsilon_a > \varepsilon_y$ and $W_r > W_a$ we have simple plastic flow,
4. when $\varepsilon_a > \varepsilon_y$ and $W_r < W_a$ we have combined flow and fracture (i.e. plastic fracture).

These inequalities are shown schematically in Fig. 8. Deformation transitions concern movement over the boundaries of the "cross". The well-known Charpy transition in steels concerns moving from the lower left quadrant to the upper left quadrant. The size-effect in brittle fracture concerns moving from the lower right quadrant to the lower left quadrant as the body increases in size and from the lower right quadrant to the upper right quadrant when the body becomes small. Vice versa, limiting sizes in comminution trace the reverse route, i.e. lower right to lower left when the particles are large and break down, but lower right to upper right when the limiting size has been reached. Similar considerations apply for the thickness requirement in plane-strain fracture toughness ($K_{IC}$) testing. Hydrostatic compression applied to brittle rocks causes the deformation to fall in the upper left quadrant (or even upper right) in place of the usual lower left quadrant. Vice versa, notch brittleness caused by hydrostatic tension at notch roots in otherwise ductile solids occurs in the lower left quadrant instead of the upper right. (Simply brittle solids remain in the lower left quadrant, and simply ductile solids in the upper right quadrant, and are unaffected by the plastic constraint of the notch.)

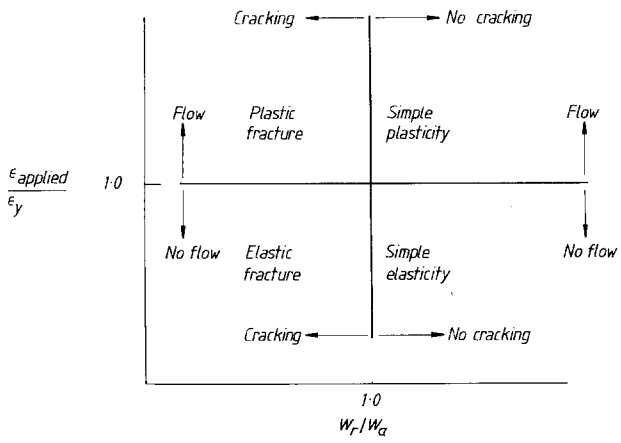


*Figure 8* Deformation transition regimes.

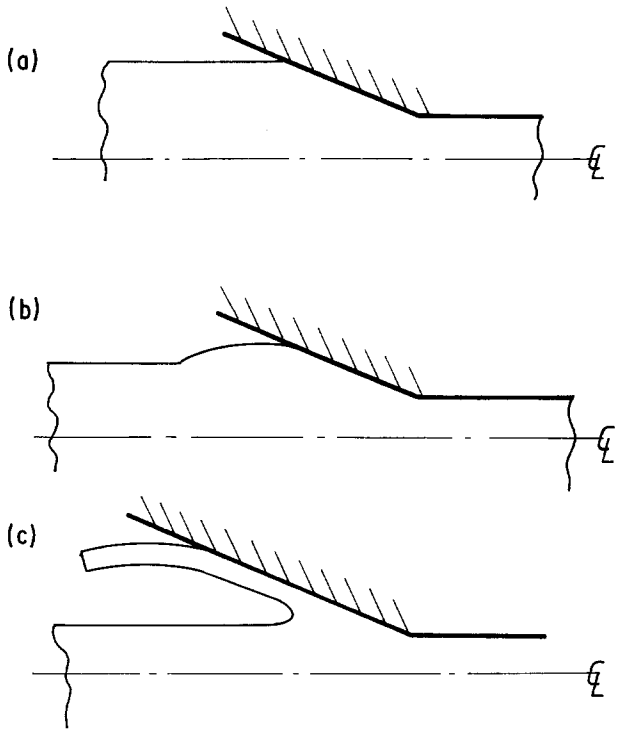


*Figure 9* Difference between (b) ironing/bulging and (c) negative-rake machining processes.

"Semi-brittle" solids sit on the boundaries of the cross. Transitions from normal wire-drawing of a ductile metal to the formation of a bulge ahead of the drawing die to the "scalping" of chips from the surface of the undrawn rod, concern moving to the left from the right in the upper part of the diagram (Fig. 9). High-density polyethylene prefers to flow in air rather than crack, but in water or other liquid environments, elastic fracture occurs (upper right to lower left). Ashby deformation-mechanism and fracture-mechanism maps for the same solid may be viewed together to show transitions from flow to fracture and vice versa [32]. For example, at a fixed temperature, the relative values of vertical stress intercepts will indicate likely events; alternatively, at fixed applied stress, horizontal intercepts will indicate transitions with temperature. Since fracture events are often controlled by energies, Ashby maps could usefully have a third axis of strain to give flow and failure surfaces.

Load–displacement, *Xu*, diagrams are displacement reversible in the lower half of Fig. 8 but are displacement irreversible in the upper half. In the lower left quadrant, broken pieces may be refitted to regain the original object; in the upper left, refitting fails to reproduce the original object owing to extensive distortion and shape change.

It would be extremely useful to be able to predict quantitatively into which quadrant a given (material, geometry, applied loading) combination will finally fall (after the initial elastic response which all bodies display). With that information it would be possible either (a) to avoid moving into an undesirable region or (b) to ensure that deformation takes place in a favoured region. The material properties which are likely to influence the behaviour are the yield strength $\sigma_y$, the Young's modulus, $E$, and the resistance to

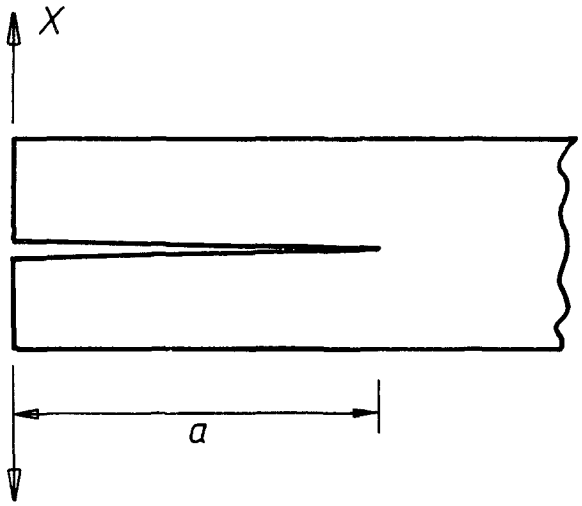


*Figure 10* Elementary DCB testpiece.

cracking (given by a variety of parameters, depending on the circumstances, such as the fracture toughness, $R$, the critical stress intensity factor, $K_c$ (which includes $E$ of course), the critical crack opening displacement, $\delta_c$, specific essential work of initiation, $J_i$, etc.). Geometrical effects, and differences in applied loading, are represented by two inter-linked parameters, i.e. (i) some characteristic length, which may be the length of a pre-existing crack or the size of the body (in elastic fracture mechanics formulae these are connected by $a/D$ ratios), together with (ii) a factor related to the level of strain in the resulting deformation field.

For illustrative purposes, consider a DCB testpiece loaded by end forces (Fig. 10). In the elastic quadrant of Fig. 8 the maximum applied stress is located at the root of the cantilever and is given by "$My/I = Xay/I$" from bending theory where $M = Xa$ is the bending moment, $a$ is crack length, $y$ is distance from the neutral axis and $I$ is second moment of area of the beam cross-section. As the ratio $\varepsilon_a/\varepsilon_y = \sigma_a/\sigma_y$ so long as the deformation is elastic, we have

$$\varepsilon_a/\varepsilon_y = Xay/I\sigma \tag{2}$$

This defines the horizontal arm of the cross in Fig. 8. The *lower* part of the vertical boundary is obtained as follows: $G = -(\partial\Lambda/\partial A)_u = X^2a^2/EIB$ so

$$W_r/W_a = R/G = REIB/X^2a^2 \tag{3}$$

The *upper* part of the vertical boundary, (for ductile fracture by void coalescence and growth for example), is defined by

$$W_r/W_a = D^*/\int(\sigma_H/\bar{\sigma})d\bar{\varepsilon} \tag{4}$$

where $D^* = \ln(l/2r)$ the McClintock damage function, with $l$ the spacing between voids of radius $r$, or some other criterion for a different micromechanism of plastic fracture [19].

Thus, armed with material properties ($E$, $\sigma_y$, $R$, $D^*$ and so on) and the value of $X$ applied, we may decide *ab initio* the response of this particular type of specimen with geometrical details ($a$, $B$, $h$).

When $\varepsilon_a = \varepsilon_y$ on the outside of the beam arms, it follows that $h = 3ER/\sigma_y^2 = 3(K_c/\sigma_y)^2$ since $y = h/2$, $I = Bh^3/12$ and $X^2a^2 = REIB$. For $h$ smaller than this, specimens will yield before fracture. We have thus identified quantitatively, at least for the double cantilever beam (DCB) geometry, the size-related transition between elastic fracture and plastic flow. The reader may recollect that functions of $ER/\sigma_y^2 = (K_c/\sigma_y)^2$ appear in various size restrictions in ASME codes for elastic fracture testing [19]. Again the size of crack tip zones in elastic fracture depends on $K_c/\sigma_y$ [33].

We note that the two separate ratios $\varepsilon_a/\varepsilon_y$ and $W_r/W_a$ seem to be combined into one lumped parameter involving $ER/\sigma_y^2$ and $h$. In fact

$$ER/\sigma_y^2h = (W_r/W_a)(\varepsilon_a/\varepsilon_y)^2 \tag{5}$$

The proof follows from multiplying both sides of Equations 2 and 3 i.e.

$$\left(\frac{REIB}{X^2a^2}\right)\left(\frac{Xay}{I\sigma_y}\right)^2 = \frac{3RE}{h\sigma_y^2} \tag{6}$$

using $I = Bh^3/12$ and $y = h/2$. Values of $ER/\sigma_y^2h$ thus correspond with *areas* in Fig. 8.

While we have determined whether merely plasticity or elastic fracture occurs first in this problem, we have not explored all possibilities. In particular we have not determined whether the initial plastic flow develops to only a limited extent before fracture still occurs, or whether the plastic flow becomes extensive before eventual fracture, or whether plastic collapse occurs with no fracture. It may be shown that if $h < ER/\sigma_y^2 = (K_c/\sigma_y)^2$ a rigid-plastic beam will form a hinge and collapse and (in the absence of work hardening) simply curl up with no fracture whatsoever. For $3ER/\sigma_y^2 > h > ER/\sigma_y^2$, the beam will fracture after prior elastoplastic bending.

In addition, then, to the transition between elastic fracture and elastoplastic flow, there is a *second* transition between elastoplastic fracture and plastic collapse. In terms of strains, the second transition corresponds (in the case of a perfectly plastic solid) with $\varepsilon_a/\varepsilon_y = \infty$.

Puttick in a series of papers in the late 1970s [34] termed the two transitions the lower transition (elastic to elastoplastic) and the upper transition (elastoplastic to fully plastic). We may write generally

$$h \gtrless \alpha ER/\sigma_y^2 \tag{7}$$

with different values of $\alpha$ for the lower and upper transitions. Clearly there are critical lengths or sizes ($h$, $D$ etc.) at which transitions occur in given geometries, which depend on the product of a material factor ($ER/\sigma_y^2$) and test geometry factors, $\alpha$.

Calculations of $\alpha$ for the lower transition are, in principle, readily performed as the critical lengths (being those of the elastic strain energy fields) are given in linear elastic fracture mechanics by the characteristic lengths of the stress fields (i.e. via the $Y(a/D)$ factor). For example, in the case of centre-cracked plates it may be shown that $\alpha = 4$ at $a = D/4$, by equating the nett-section stresses at elastic cracking (i.e. $K_c/[D\tan(\pi a/D)]^{1/2}$) to the yield strength $\sigma_y$ over the same ligaments.

Calculations for $\alpha$ at the upper transition are less reliable as elastoplastic solutions for cracking problems are formidable and usually not available.

This is so for elastic-perfectly plastic solids and further complications are introduced by workhardening.

In the absence of a proper solution, one approach for $\alpha$ at the upper transition is to consider the size of the crack tip zone and enquire when it may reach an outside boundary of the cracked body. Consider first the size of the crack tip zones at the *lower* transition in a centre-cracked plate (CCP). For $a/D = 0.25$ and with $K_c = \sigma_y[D \tan(\pi a/d)]^{1/2}$, the size of the crack tip zones is $d_y = (1/\pi)(K_c/\sigma_y)^2 \approx 0.08D$ in plane stress and about $0.03D$ in plane strain [33]. The crack tip zone size, as a proportion of the crack length ($2a = 0.5D$) is $0.08D/0.5D = 0.16$ (plane stress) and some $0.03D/0.5D = 0.6$ (plane strain). While the latter size is greater than that recommended for plane strain testing* (i.e. ratio $\approx 0.02$), the zones are still contained within the extent of the nett section ligament ($0.25D$ on each side of the crack). However, were the extent of the crack tip zone to reach an outside boundary of the crack body, this would correspond with the upper transition. Hence for CCP with $a/d = 0.25$ and a $0.25D$ ligament between the starter crack tip and the free boundary of the specimen, $d_y$ equals $0.25D$. Thus, we have

$$(1/\pi)(ER/\sigma_y^2) = 0.25D$$

or

$$d < (4/\pi)(ER/\sigma_y^2) \quad (8)$$

so that for the upper transition, $\alpha = (4/\pi)$.

This type of calculation is crude, as it assumes that the crack tip zone is circular when in fact it may be lobe-shaped or take the form of a Dugdale-type line zone [33], and may also depend on strain rate, the form of the yield criterion and so on. Furthermore, and for related reasons, alternative lines of attack (e.g. in terms of loads or stresses) for the upper $\alpha$ do not always give the same answer.

Table I (taken from Atkins and Mai [19]) gives lower and upper $\alpha$ values for a number of different geometries. We see from the table that situations with compressive major principal stresses (e.g. Hertzian indentation) require large critical characteristic sizes at the transitions, i.e. large $\alpha$. The lowest values of $\alpha$ are associated with tension stress fields in notched bars which experience high $\sigma_H$ and hence promote fracture.

In the general workhardening case, it is difficult to assign a level for $\varepsilon_a/\varepsilon_y$ which would give a second horizontal line for the upper transition in Fig. 8. Sometimes the plastic zone comprises a field of not-too-large plastic strains diffused over a wide region, but at other times high strains may be concentrated in a small volume (cf. shear cutting processes); in both cases, however, the total incremental plastic work done in the deformation could be comparable with each other and with the work of fracture. Even so, we may qualitatively refine Fig. 8 to accommodate both the lower and upper fracture transitions, as shown in Fig. 11 where the plastic flow, $\varepsilon_a/\varepsilon_y$, ordinate is labelled "none", "limited" and "extensive". It may also be possible to think in terms of "limited" and "extensive" cracking on the abscissa too.

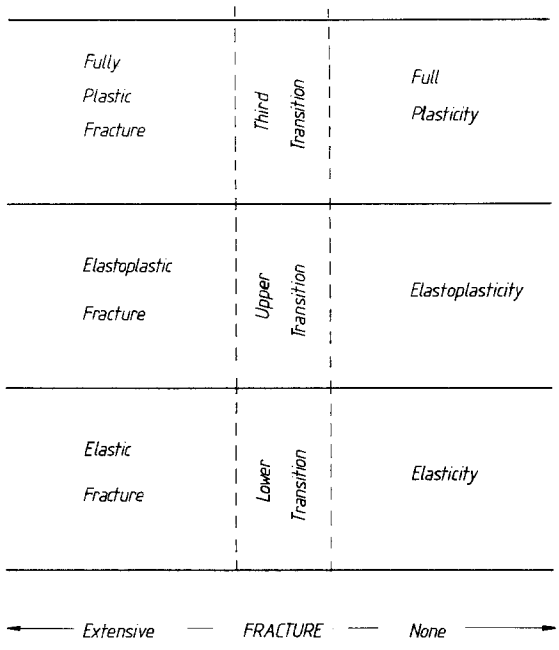


*Figure 11* Upper, lower and third transitions for fracture and plastic flow.

We are now in a position to re-examine Ludwik's postulate of a size-independent fracture curve for all types of specimen of a given material. As $\sigma_f^2 = ER/Y^2\pi a$, where $Y$ is a constant for a give type of specimen, we see that $\sigma_f$ is *not* constant for a given material, even if inherent flaw sizes are the same in different specimens, owing to changes in $Y$. Likewise, the fracture strengths of brittle solids ("moduli of rupture" in bend tests) will depend on specimen geometry and size; equally "compressive fracture strengths" of notched or plain specimens (which are based on local tensile fractures, as in the Brazilian disc test for rocks [36]) will depend on specimen geometry. The fundamental parameter in these sorts of measurement is not fracture stress, but specific work of fracture ($R$).

Again, susceptibility to notch-brittleness depends on the relative values of $\sigma_y$, $(1/Y)(ER/\pi a)^{1/2}$, and $3\sigma_y$. That is, a simply brittle solid has $ER/\sigma_y^2 < Y^2\pi a$, a simply ductile material has $ER/\sigma_y^2 > 9Y^2\pi a$, and a notch brittle solid has $ER/\sigma_y^2$ in between. $(1/Y^2\pi)$ and $(1/9\,Y^2\pi)$ correspond with $\alpha$ for the lower and upper transitions, respectively. Knowing the appropriate $Y^2a$ for a chosen type of testpiece permits the value of $ER/\sigma_y^2$ for the solid to be bracketted and different types of notched specimen can, in principle, refine the answer. This was a useful concept (like UTS/$\sigma_y$ ratio) years ago to quantify "toughness" but these days $K_c$ or $R$ is measured independently from standard toughness tests and rarely from notch brittleness tests.

A number of different physical interpretations may be put on the $ER/\sigma_y^2$ or $ER/\sigma_y^2 h$ parameters. In the DCB specimen $ER/\sigma_y^2 h = (K_c/\sigma_y)^2/h$ represents the

*Experiments show that measured values of $K_c$ in centre-cracked panels are affected by impending general yield in the ligament (Kenny and Campbell [35]. It is recommended that the nett section stress be kept below $0.8\sigma_y$ for displacement-reversible cracking; this reduces the size of the crack tip zones towards recommended values. A limiting size of zone, as a proportion of crack length, is an alternative way of setting $\alpha$ values for the lower transition.

TABLE I

| Process | Lower transition elastic-electoplastic | Upper transition elastoplastic-fully plastic |
|---|---|---|
| Ball indentation | $\alpha \approx 2300\,ER/\sigma_y^2$<br>$a$ = radius of Hertz ring crack<br>(friction and slip at interface reduces $\alpha$ to around 200 for steel ball)<br>*also*<br>$a \approx 100\,ER/\sigma_y^2$<br>for yielding directly beneath ball during later growth of cone crack. | $a = 15\,ER/\sigma_y^2$<br>$a$ = impression radius *or* equivalently<br>$c = 25\,ER/\sigma_y^2$<br>$c$ = plastic zone radius around identation |
| Embedded rod | $d = 8\,ER/\sigma_y^2$ | $d = 8\,ER/(\mathrm{UTS})^2$ (necking) |
| Unloading indentation cracks (residual stress fields) (scratching) | $\alpha \approx 6\,ER/\sigma_y^2$ | |
| DCB compression (comminution) | $d \approx (32/3)\,ER/\sigma_y^2$ | |
| Centre-cracked plate | $W \approx 4\,ER/\sigma_y^2$<br>$(a = W/4)$ | |
| DCB | $h \approx 3\,ER/\sigma_y^2$ | $h \approx (4/3)\,ER/\sigma_y^2$<br>or<br>$h \approx (1/2\pi)\,ER/\sigma_y^2$ |
| Glued Elastoplastic beam | $h = 3\,ER/\sigma_y^2$ | $h = RE/\sigma_y^2$ |
| 3-point bending, Charpy | $W \approx ER/\sigma_y^2$ | $W \approx 0.15\,ER/\sigma_y^2$ |
| Deeply edge-notched plate | $W \approx 0.8\,ER/\sigma_y^2$ | $W \approx 0.1\,ER/\sigma_y^2$ |
| Machining (fragmentation-to-curly chip formation) | $h = 0.6\,ER/\sigma_y^2$ where $h$ is depth of cut | |
| Guillotining (ductile metals) | | $\delta_{cr}^{n+1} = Rw^n/\tau_0\left[\frac{1}{n+1} - f\right]$<br>$\delta_{cr}$ critical depth of indentation; $w$ width of shear zone<br>$n$ workhardening index<br>$\tau = \tau_0\gamma^n$<br>$f$ friction factor |

ratio of cracking force to the force required to produce plastic flow. The relevant lower and upper $\alpha$ values determine whether the flow is limited or extensive, i.e. $\alpha$ for the lower transition is larger than $\alpha$ for the upper, so as $ER/\sigma_y^2 h = 1/\alpha$, this is the same as saying that cracking will occur if the force to crack is lower than the force to yield. This approach has been useful in consideration of transitions in machining [37, 38].

Another interpretation is that $ER/\sigma_y^2 = \delta_c/\varepsilon_y$ where $\delta_c$ is the critical opening displacement. This follows from writing $R \approx \sigma_y \delta_c$. This particular meaning is employed in the crack opening displacement (COD) design curve [31, 39] (but note that in that code of practice $\delta_c/\varepsilon_y = 2ER/\sigma_y^2 = 2(K_{IC}/\sigma_y)^2$ with a deliberately built-in safety factor of two). Size transitions given by Equation 7 can be rewritten as:

$$h \gtrless \alpha(\delta_c/\varepsilon_y). \tag{9}$$

This may sometimes be a more convenient way of establishing $\alpha$, particularly at the upper transition. Hence even materials with large $\delta_c$ can still behave in a globally elastic reversible fashion if $h$ is big enough, but the large $\delta_c$ inevitably has to be accommodated in an extensive plastic field if $h$ is small. Clearly the situation is changed in different crack geometries (different $\alpha$): when $\alpha$ is small (at notch roots in tensile specimens) elastic fracture occurs in smaller specimens, other things being equal.

There is a third value of $\alpha$ which determines when, in a given geometry, plastic fracture supervenes plastic flow. As illustrated schematically below, the three values of $\alpha$ determine the behaviour when successive choices have to be made between (a) elastic to either fracture or elastoplastic flow; (b) elastoplastic flow to either elastoplastic fracture or plastic flow; and (c) plastic flow to either plastic fracture or unlimited plastic flow.

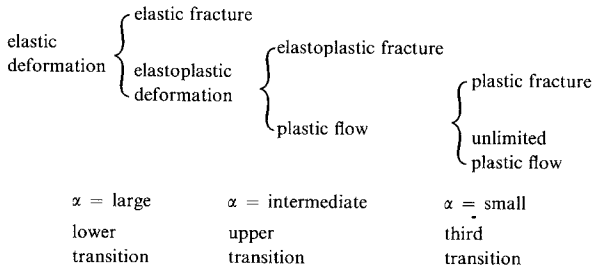


The trend in Fig. 11 is that the transitions are set by critical values of $ER/\sigma_y^2 h = 1/\alpha$, and that $1/\alpha$ is smallest for the lower transition, larger for the upper transition and (if it can be used) presumably largest for the third transition. Of course, it may be argued that the third transition is meaningless as all materials will eventually fracture as the level of deformation is increased unless they have peculiar (time-dependent) flow properties. Information that the third transition does supply, though, is the level of extensive large-strain plastic deformation which precedes fracture.

Fig. 12 presents the transitions in terms of the diagram (Fig. 6c) used to explain the size effect in

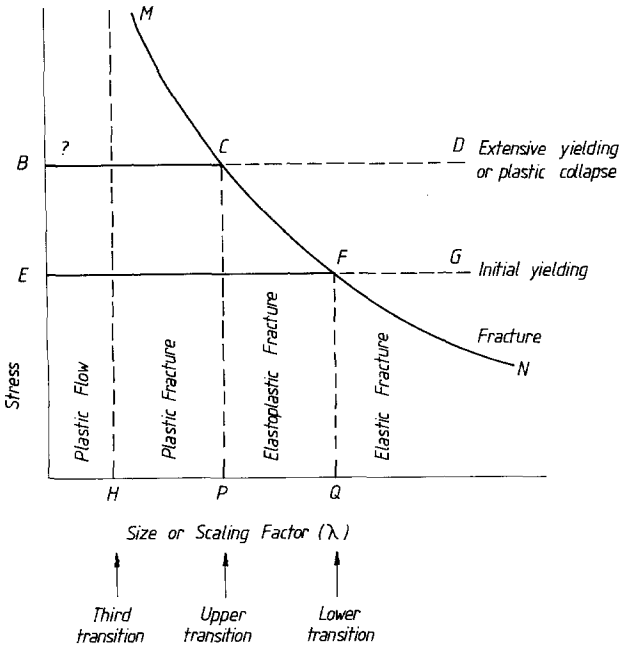


*Figure 12* Size effect in fracture incorporating lower, upper and third transitions.

Section 2.1. There are now two stress levels for plastic flow, one EFG for initial yield and a second BCD for extensive yielding (which corresponds with unlimited plastic flow or collapse in a rigid-perfectly plastic solid). It is not obvious how to set the level of BCD in a workhardening solid. One point of view is to say that BCD corresponds with the least stress level at which the plastic zones reach an external boundary of the cracked body. The fracture stress curve M . . . N will be given by the appropriate algebra for the fracture stress at *all* sizes, i.e. which expresses elastic fracture, elastoplastic fracture and plastic fracture.

There are hardly any closed-form solutions for fracture loads covering the whole range of transitions. One example, however, relates to the adhesive fracture of a beam glued to a massive substrate (Figs. 13a and b) in which the possible plastic flow in the beam may be uncoupled from the fracture events along the glue line. (In cohesive fracture of monolithic solids, the separation of these events, and the interpretation of unloaded work areas after some propagation into components of plastic work, fracture work and residual elastic strain energy is formidable and the subject of much debate [40].) Let us define the "fracture stress" for this problem as $(X/wh)$ where $w$ is the width of the beam and $2h$ its depth, with $X$ the equivalent end-load which, with a cantilever length $a$, gives the cracking moment $M = Xa$. Then, for elastic fracture [19]

$$X/wh = [4RE(h/a)/3]^{1/2}(1/a^{1/2}) \qquad (10)$$

and for elastoplastic fracture

$$X/wh = (h/a)\sigma_y\{1 - (3/4)\{1 - RE/\sigma_y^2(h/a)(a)]^2\} \qquad (11)$$

In both cases, for geometrically similar specimens where $h/a$ is constant (assumed for simplicity) the fracture stress diminishes as the "size" (represented by $a$ here) increases and the fracture stress curve falls from left to right in Fig. 12.

It is clear that intersection points F and C in Fig. 12 between the fracture stress and flow stress curves, correspond with Puttick's lower and upper transitions. The fracture stress curve is continuous through point F, with the portion NF being given by Equation 10 and portion FC by Equation 11. At point F, $(X/wh) = 2RE/\sigma_y a$ by both relations. For rigid-perfectly plastic solids, the portion CM does not exist in theory as an unlimited rotation occurs to the left of point C. For practical work-hardening solids, CM does exist, if BC is considered (in this beam problem) simply as the stress level at which the whole beam depth is encompassed by plastic flow. The algebra for portion FC of the fracture stress curve may be viewed as the algebra for the *elastic* curve, but with a progressively changing "enhanced" or "apparent" toughness, $R^*$, given (for the beam problem) by $R^* = R(3 - \xi^2)^2/4(3 - 2\xi)$ where $\xi$ defines the extent of the plastic zones in the beam [19]. It is likely that many elastoplastic cracking problems may, in general, be viewed in this way where the connexion between $R^*$ and $R$ depends upon process zone size, accompanying irreversibilities inherent to propagation in a given geometry and so on; the result is clearly relevant to Andrews' multiplicative approach to elastoplastic fracture [41].

Hence, in broadest terms, the fracture stress will usually have the shape given in Fig. 12 and the following conclusions may then be drawn:

1. As the stress is increased in a body where $\lambda > \lambda_Q$, the portion FN of the fracture curve

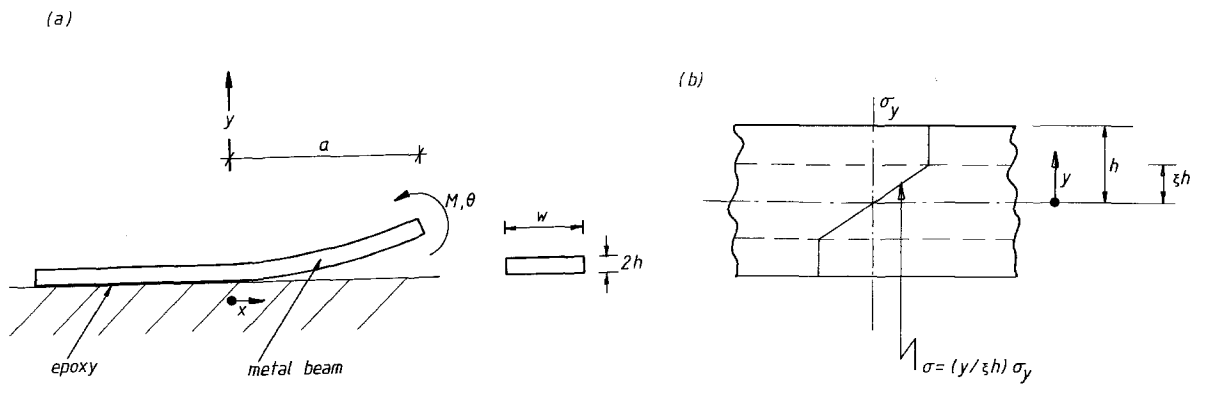


*Figure 13* (a) Peeling of an elastoplastic metal–epoxy joint by an end couple and (b) stress distribution across the beam depth showing the regions of elastic and plastic bending.

is intersected first and hence elastic fracture ensues.

2. For a body in which $\lambda_P < \lambda < \lambda_Q$, the initial yielding boundary is intersected first, followed by the fracture curve between C and F. For bodies with $\lambda_H < \lambda < \lambda_P$, initial yielding is followed by extensive yielding and eventual fracture on the MC boundary.

3. If $\lambda_H$ exists, and $h < \lambda_H$ it seems that unlimited flow can take place with no fracture at all. The position of H would be such that the fracture curve NFCM would be asymptotic to a vertical line through H.

The fracture stress required for propagation, and the stresses associated with yielding, may change as propagation ensues which means the boundaries may change and the events may change. For example, plastic flow may occur after some elastic fracture propagation in ligaments in the path of the crack, which obviously decrease in size as cracking progresses. Questions of non-proportional scaling, crack stability, rate, temperature and environment all come into play in the full interpretation of events in Fig. 12 and clearly, alteration of any one variable in the lumped parameter $\alpha ER/\sigma_y^2 h$ may put the deformation into different regions of Figs. 8 or 11.

Some numerical solutions for some transitions are contained in the Appendix. In all cases the behaviour may be expressed in terms of versions of Equation 7, i.e. $h \gtrsim \alpha ER/\sigma_y^2$.

## 4. Deformation transitions and design

We have seen that a body, when loaded, may behave merely elastically; may crack elastically; may behave elastoplastically, may crack in the elastoplastic regime; may experience widespread plastic flow; or may fracture after extensive remote flow. Which (if any) of these various possibilities constitutes "failure" to an engineering designer? The answer clearly depends upon the purpose of the component or structure being designed, its size and shape, the loading, and the material from which it is made.

Most traditional design relates to the elastic range of deformation with, usually, high structural loading coefficients (i.e. comparatively high loadings over the extent of the body) using stiff materials: in contrast tents, pneumatic structures and the like, and many natural structures (plants and animals) have low structural loading coefficients and low stiffness materials. Traditional design is based on a safety-factored yield stress, employing "ductile" materials. It is an acceptable design philosophy, particularly in relatively small, well-manufactured components and structures, and relates to keeping the working stresses below line EF in the HP size range of Fig. 12 for monotonic loadings. If the article is defective (cracks, bad welds, and so on) unexpected failures can occur. But deformation transitions, produced by increased size of components and structures, led to brittle fractures (FN line in Fig. 12) in even well-manufactured bodies, and hence to the birth of modern elastic fracture mechanics in order to explain these unexpected failures and to design against them. Furthermore, the ability to perform "strength-of-materials" elastic calculations for *cracked* bodies (for that is what LEFM is all about as far as a designer is concerned) has permitted the use, in some applications, of high strength materials whose $K_c/\sigma_y$ ratios are relatively much lower than the traditional ductile solids of engineering design; use of these materials implies appropriate crack inspection procedures. Of course, an application of fracture mechanics principles is central to design with brittle materials such as glasses and ceramics whose $K_c/\sigma_y$ ratios are very low indeed.

Design rules for material/geometry/size combinations in the region from the origin to P, and in the region beyond Q, in Fig. 12, seem to have been covered therefore, i.e. yielding or plastic collapse in the first case and reversible elastic fracture in the other. What of the region PQ in between, in which elastoplastic fracture is possible, i.e. cracking after only limited irreversible flow? This is difficult: if plasticity is not very extensive (just to the left of point Q, say) the $J$-integral approach [42] may be used; alternatively, the COD design curve may be used [39]. However, if design concerns the region of the diagram just to the right of P, the solution is not clear and is the subject of current research.

One approach to the problem is to *bound* the answer by LEFM and limit analysis. Crack initiation may precede overall yielding or vice versa. Hence LEFM and limit analysis will provide either upper or lower bounds depending on the circumstances, i.e. in Fig. 12 line MCFN or line BCD may be reached first, depending on where on the abscissa the particular material/size/cracked geometry combination lies. Ruiz and Corran [43] draw the analogy of the design of a strut with the safe design of a structure containing a flaw: with a strut, the possibilities of either Euler crippling or plastic squashing have to be considered; design against the failure of a structure made of material with intermediate-to-high $K_c/\sigma_y$ and possessing flaws needs consideration of fracture in the elastic field, on the one hand, or general yielding on the other. That the possibility of plastic flow may be as important (or more important) a consideration as elastic fracture in these circumstances is borne out by the observations of Soete in 1977 [44] who noted that the safety of structures built with ordinary commercial steels depends more on their plastic properties than on their fracture toughness (i.e. extensive yielding nearly always precedes fracture). Furthermore, Ruiz [45] showed that ductile crack growth in cracked cylindrical shells can, in fact, be predicted by limit analysis alone, i.e. the predicted pressure to cause widespread yielding in the presence of longitudinal notches or through-thickness slits agrees with reported experimental "failure" pressures in pipelines and boilers made of medium-to-high $K_c/\sigma_y$ materials. LEFM and related analyses were not appropriate.

It is clear that deformation transitions are central to the use of extremal elastic and fully plastic solutions for the design of structures made from materials possessing high $K_c/\sigma_y$ ratios, and also for the assessment of defects in such structures, i.e. what cracks may be tolerated *vis à vis* realistic levels of inspection. Fig. 14 is taken from Corran *et al.* [46] and illustrates

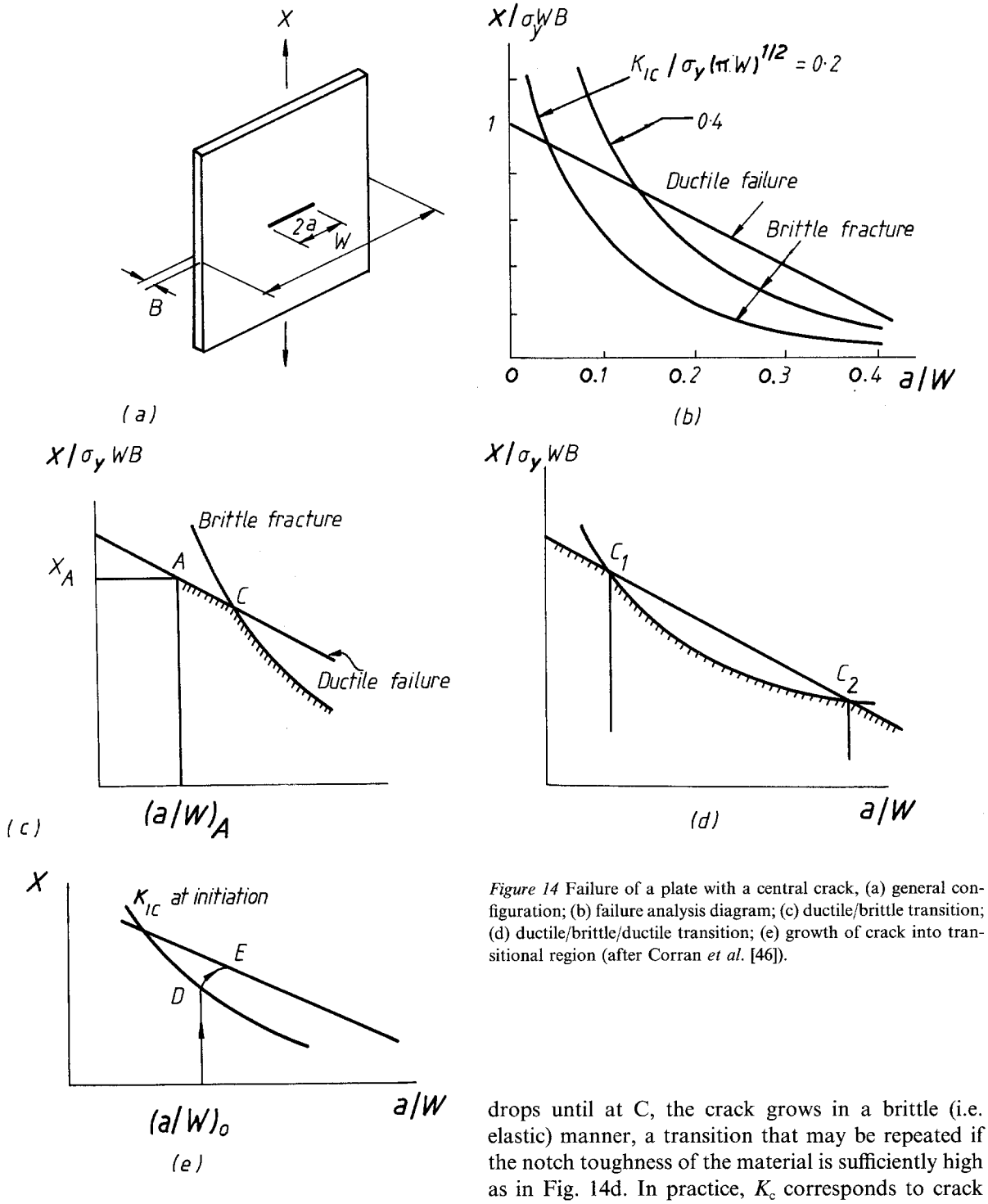


*Figure 14* Failure of a plate with a central crack, (a) general configuration; (b) failure analysis diagram; (c) ductile/brittle transition; (d) ductile/brittle/ductile transition; (e) growth of crack into transitional region (after Corran *et al.* [46]).

the competition between fracture and flow for a centre cracked panel. Elastic fracture occurs when $\sigma(\pi a)^{1/2} = K_c$, where $\sigma \approx X/B(W - 2a)$ where $W$ is the width of the plate. Assuming the material to be rigid-perfectly plastic with flow stress $\sigma_y$, plastic collapse in plane stress occurs when $X = \sigma_y B(W - 2a)$. These two relations for $X$ (normalized by $\sigma_y BW$) are shown in Fig. 14b, the former for two values of $(K_c/\sigma_y(\pi W)^{1/2})$. The intersection between the "ductile failure" line and the "brittle fracture" curve corresponds to the transition between the two modes of failure, governed by ductile (limit analysis) behaviour to the left of the intersection and by brittle (LEFM) behaviour to the right. Note the similarity of the diagram to Fig. 12. Thus, in Fig. 14c, a plate with a small defect, at A, will first yield as the load reaches $X_A$. As the crack grows, reducing the net cross-sectional area, the applied load drops until at C, the crack grows in a brittle (i.e. elastic) manner, a transition that may be repeated if the notch toughness of the material is sufficiently high as in Fig. 14d. In practice, $K_c$ corresponds to crack initiation and, depending on the loading condition, strain rate and plastic constraint, failure within the brittle region $C_1C_2$ of Fig. 14d may take place as illustrated in Fig. 14e: a crack of initial length $(a/W)_0$ starts growing at D, along the path DE in the transitional region until at E fully plastic behaviour sets in. The various intersection points correspond with Puttick's $\alpha$ equalling $(1/\pi)$ in value, that is, when $\sigma = K_c/(\pi a)^{1/2} = \sigma_y$, $a = (1/\pi)\,(K_c/\sigma_y)^2$.

The investigations of Ruiz and co-workers [46] into the elastoplastic behaviour of compact tension specimens of maraging steel ($K_c/\sigma_y \approx 0.1\,\mathrm{m}^{1/2}$) and polycarbonate ($K_c/\sigma_y \approx 0.07\,\mathrm{m}^{1/2}$) show that although crack initiation is predicted by LEFM, the maximum load is predicted by limit analysis; and that in specimens with relatively large cracks, in which substantial plastic deformation precedes cracks initiation, the two approaches coincide. (To account for practical

strain hardening in such analyses it is customary to use $(\sigma_{UTS} + \sigma_y)/2$ or some such in place of $\sigma_y$). Corran *et al.* [46] applied the results to model flawed cylindrical pressure vessels made from polycarbonate. They obtained excellent agreement between theory and experiment – pressure against crack growth diagrams following the shape of Fig. 14e when failure was by widespread yielding which occurred with small vessels; of note, a set of large model vessels failed in a brittle manner, which accords with the size effect shown in Fig. 12.

Of course, extremal solutions provide only independent estimates for the two limits to the initiation of "failure", i.e. brittle fracture or widespreading yielding. (Fracture subsequent to widespread yielding, i.e. the third transition of Section 3, is not usually considered in this type of structural calculation). Bounding solutions give no indication of the transitional behaviour, and (when formulated in terms of rigid-perfectly-plastic collapse) do not account for workhardening deformation. Dowling and Townley [47] proposed to combine the two extremal solutions, establishing an interaction diagram, which leads to the CEGB "two-criteria" approach for design (sometimes called the R-6 failure assessment procedure). Plasticity is that associated with a Dugdale zone extending ahead of the crack tip, and (although not actually presented this way originally) degrees of elastoplastic fracture may be visualized to arise from what proportion of a remaining ligament ahead of the crack is taken up by the Dugdale zone. The diagram has axes of

$$K_r = \frac{K_c[a, X, Y(a/D)]}{K_{IC}}$$

and

$$S_r = \frac{X}{X_c} \qquad (12)$$

for the ordinate and abscissa, respectively. For a given crack geometry, and a given loading condition, the diagram identifies how close the situation is to either elastic fracture, elastoplastic fracture or plastic collapse. The diagram is a useful means, therefore, of assessing the safety margin of a flawed structure. Developments of the R-6 diagram permit thermal and residual stresses, and slow crack growth to be incorporated. There is some debate about the detail of the diagram (see, for example, [46]) and how the separate fracture and flow events are blended-in.

Owing to the closed-form solution of the elastoplastic glued beam problem mentioned in Section 3, it is possible to construct an *exact* elastoplastic interaction diagram for this particular problem. For elastoplastic deformation of the beam coupled with fracture along the glue line (i.e. fracture in the transition region between elastic fracture and plastic collapse), we have [19] $M^2 = (REIw/2)(3 - \xi^2)^2/(3 - 2\xi)$. The moment when the beam just remains completely elastic, i.e. $\xi = 1$ is $M_{el}^2 = 2REIw$. For the purpose of the diagram, the ordinate is $M/M_{el}$ and we see that $(M/M_{el})^2 = (3 - \xi^2)^2/4(3 - 2\xi)$. This expression must be transposed so that the function of

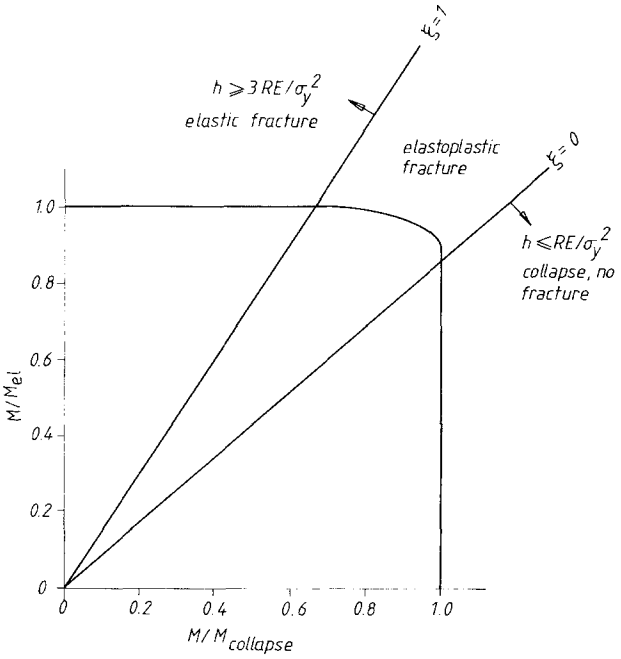


*Figure 15* Exact "R6" interaction diagram for glued cantilever beam problem.

$\xi$ becomes a function of $M/M_{collapse}$. Now $M_{collapse} = wh^2\sigma_y$, and from [19] an alternative expression for $M_{elpl}$ is $wh^2\sigma_y(3 - \xi^2)/3$. Thus $M/M_{collapse} = (3 - \xi^2)/3$ and $\xi^2 = 3(1 - M/M_{collapse})$. Substituting back for $\xi$, and calling $M/M_{el} = y$ and $M/M_{collapse} = x$, we have $y^2 = 9x^2/4\{3 - 2[3(1 - x)]^{1/2}\}$ as the equation of the interaction diagram. Fig. 15 gives the plot. Note that $M/M_{el} = 1$ until $M/M_{collapse} = 2/3$ (for rectangular beams). The interaction curve corresponds with $\xi$ changing as shown. The bounding radial lines for $\xi = 0$ and $\xi = 1$ give Puttick's lower and upper transitions in this problem.

## Appendix

Calculations for the $\alpha$ values in $h \gtrless \alpha(ER/\sigma_y^2)$ which determine transitions are given as follows. Values of $\alpha$ in Table I were obtained in these sorts of ways.

### A1. Spot welds

Fig. 5 shows Smith's comparison between experiment and theory [48]. Failure occurs either by cracking across the weld junction (at low loads) or by pulling out a plug of ductile metal in shear at higher loads. Interfacial fracture occurs at small weld diameter-to-sheet thickness ($d/B$) ratios, and vice versa for plug formation. For small ($d/B$) and low loads, deformations are small, the initial geometry is maintained, and elastic fracture may be modelled as a sharp circular neck surrounding the embrittled weld nugget and heat-affected zone. The stress intensity factor formula employed was

$$K = 0.8\,XB/d^{5/2} \qquad (A1)$$

which is an appropriate simplification of a more complicated expression. Hence

$$X_{crack} = 1.25\,K_c d^{5/2}/B \qquad (A2)$$

For "failure" by shear around the *two* circumferential

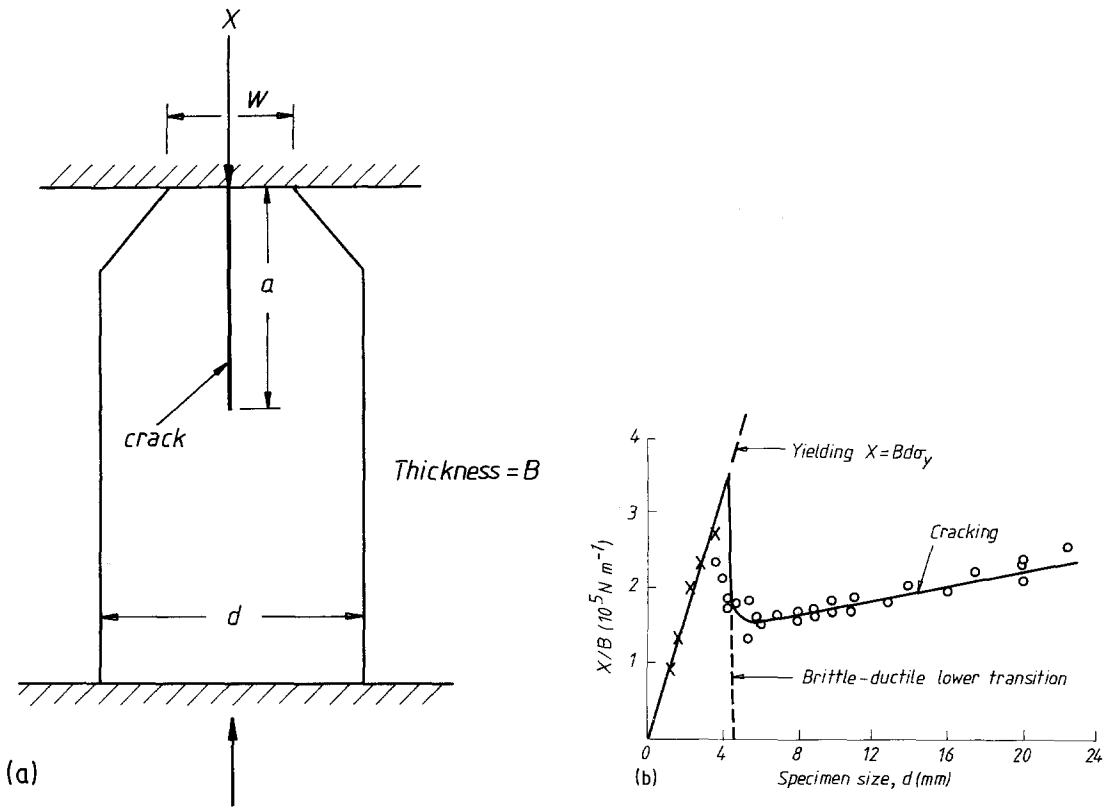


*Figure A1* (a) Axial splitting a DCB specimen by compression and (b) compression results for a range of specimen sizes showing yielding of small samples and cracking of large ones (both after Kendall [12]).

areas (above and below the weld) we have

$$X_{\text{yield}} = 2(\pi/d)B\tau_y \quad \text{(A3)}$$

where $\tau_y$ was taken as the flow stress.

The critical weld size at the transition is given when $X_{\text{crack}} = X_{\text{yield}}$, i.e. from

$$\frac{B^4}{d^3} = 0.16\left[\frac{K_c}{\sigma_y}\right]^2 \quad \text{(A4)}$$

or

$$B = 0.16\left(\frac{d}{B}\right)^3\left[\frac{ER}{\sigma_y^2}\right] \quad \text{(A5)}$$

(taking $2\tau_y = \sigma_y$). Notice that the length dimension for Puttick's transition expression is a combination of $B$ and $d$ together, not one simple size parameter.

Fig. 5 gives Smith's comparison between the analysis and data of Rivett [49] for spot welds of 1.18 mm thick cold-rolled mild steel. The transition weld diameter was predicted to be 4.65 mm which, together with the predicted transition load of 5.1 kN, clearly separates the elastic and elastoplastic fracture modes.

## A2. Comminution

Kendall [12] used a "buckling" model of the DCB testpiece (Fig. A1a). The axial cracking force, $X$, is related to the geometry of the beam and mechanical properties of the solid by

$$X_{\text{crack}} = [B/(1 - w/d)](2ERd/3)^{1/2} \quad \text{(A6)}$$

The axial load to cause yielding is given by

$$X_{\text{yield}} = \sigma_y Bw \quad \text{(A7)}$$

where $w$ is the current width of an originally sharp edge.

The lower transition is given when $X_{\text{crack}} = X_{\text{yield}}$, i.e.

$$(1 - w/d)w = (2ERd/3\sigma_y^2)^{1/2} \quad \text{(A8)}$$

For different ($w$, $d$) size combinations, this relation gives the conditions for a lower transition.

The value of $w$ depends on the applied $X$ and the plastic flow properties given by $\sigma_y$. If $w$ is eliminated, $X_{\text{crack}}$ is seen to be governed by the following quadratic:

$$(X/B)^2(1/\sigma_y d) - (X/B) + (2ERd/3)^{1/2} = 0 \quad \text{(A9)}$$

The solution appears in two parts in Fig. A1b. For large $d$, the first term may be neglected and $X_{\text{crack}}$ depends on $d^{1/2}$, but as the particle size is reduced towards a critical value given by

$$d = 32ER/3\sigma_y^2 \quad \text{(A10)}$$

(when in the quadratic solution "$(b^2 - 4ac)^{1/2} = 0$" i.e. the cracking force rises very rapidly. Eventually it exceeds the yield stress (however high this may be) and below the critical size, cracking is impossible and flow occurs instead. We see that $\alpha = 32/3$. Fig. A1b includes Kendall's model results on polystyrene for which $E = 2.8$ GPa, $\sigma_y = 80$ MPa, $R \approx 960$ J m$^{-2}$. The critical $d$ at transitions is about 4.5 mm from the theory; the experimental transition is some 3.6 mm. Given the simplifications in the analysis the agreement is very good.

## A3. Notch bend tests

As is well-known from the Charpy test, change in

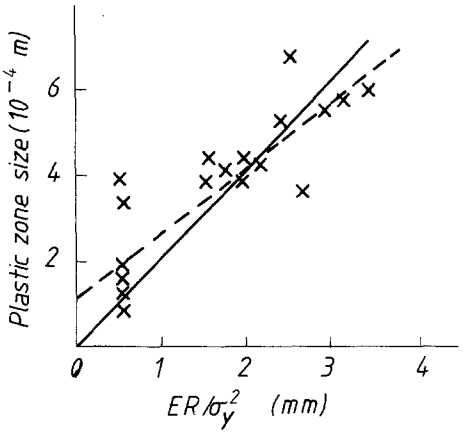


*Figure A2* Charpy notched bar fracture of silicon iron: notch root plastic zone length at fracture for values of ratio fracture load/general yield load $< 0.64$. --- Line of best fit (slope 0.15); ——— line through origin of slope 0.2 (data from Griffiths and Oates [50], after Puttick [34].

temperature is a powerful means of producing a transition, as it alters $R$ and $\sigma_y$ in steels (and would alter $E$ as well in many polymers around room temperature). Notch bend tests on silicon iron by Griffiths and Oates [50] provide evidence of the correlation between fracture transitions and the $ER/\sigma_y^2$ parameter. The fracture load, general yield load and the length of the plastic zone at the notch root (as a function of applied load/yield load) were measured at a variety of temperatures.

At 40° C, for example, the plastic zone was about 1 mm in extent and the (temperature-dependent) mechanical properties of silicon iron are: $E = 200\,\text{GPa}$, $R = 5\,\text{kJ m}^{-2}$ and $\sigma_y = 470\,\text{MPa}$. We have $ER/\sigma_y^2 = 200 = 10^9 \times 5 \times 10^3/(470 \times 10^6)^2 = 4.5 \times 10^{-3}$ m. Hence with a plastic zone size ($h$) of 1 mm, $\alpha$ for that temperature is $\alpha = 10^{-3}/4.5 \times 10^{-3} = 0.2$. The overall results in Fig. A2 show that the data follow a straight line with slope ($\alpha$) through the origin of about 0.2. The line of best fit of the experimental data is about 0.15.

## A4. Ball indentations

Fig. 3a shows (upper) transitions between elastoplastic flow in ball indentation and elastoplastic fracture caused by change in temperature. The data may be re-interpreted in terms of the relationship between the critical radius, $r_c$, of the indentation plastic zone at which at least one radial fracture was observed and $(ER/\sigma_y^2)$. As in Section A3, $ER$ and $\sigma_y$ change with temperature, and Fig. A3 shows that $r_c \approx 30\,(ER/\sigma_y^2)$; Puttick *et al.* [51], on the basis of elastoplastic analysis of ball indentation employing a pressure-dependent yield criterion for polymers, gave a theoretical value for $\alpha$ of 25.

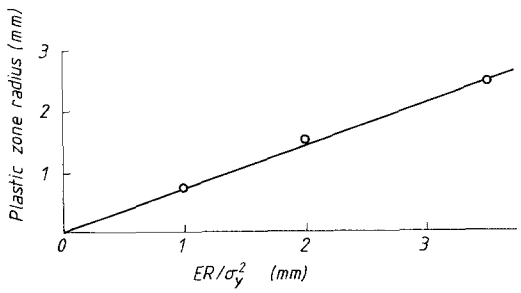


*Figure A3* Critical radius of the identation plastic zone as a function of $(ER/\sigma_y^2)$. (cf. Fig. 3a) Line of best fit gives slope of 30 (after Puttick *et al*,. [51]).

We conclude by noting that different sized balls produce different degrees of deformation and hence change the transition temperature: remember that Charpy transitions, for example, are also altered by the geometry of the notch (e.g. keyhole notches and so on).

Other correlations of size and $ER/\sigma_y^2$ relating to, for example, optical transmittance loss caused by erosion and so on may be found in Atkins and Mai [19].

## Acknowledgements

We are grateful for valuable discussions with K. E. Puttick and N. Jones.

## References

1. A. H. COTTRELL, "The Mechanical Properties of Matter" (Wiley, New York, 1964).
2. A. NADAI, "Theory of Flow and Fracture of Solids" (McGraw-Hill, New York, 1950).
3. L. E. SAMUELS, *Sci. Amer.* (1978) 132.
4. A. J. SEDRICKS and T. O. MULHEARN, *Wear* **7** (1961) 451.
5. T. C. BUTTEREY and J. F. ARCHARD, *Proc. Inst. Mech. Eng.* **185** (1970-71), 537.
6. R. W. TRUSS, R. A. DUCKETT and I. M. WARD, *J. Mater. Sci.* **16** (1981) 1689.
7. S. ROBINOWITZ, I. M. WARD and J. S. C. PARRY, *ibid.* **5** (1970) 29.
8. A. W. CHRISTIANSEN, E. BAER and S. V. RADCLIFFE, *Phil. Mag.* **24** (1971) 451.
9. D. R. MEARS, K. D. PAE and J. A. SAUER, *J. Appl. Phys.* **40** (1969) 4229.
10. J. S. TRENT, A. Y. MOET, M. J. MILES and E. BAER, *Polym. Eng. Sci.* **18** (1978) 1235.
11. F. A. McCLINTOCK and A. S. ARGON, "Mechanical Behaviour of Materials" (Addison-Wesley, Reading, Massachusetts, 1966).
12. K. KENDALL, *Proc. R. Soc.* **A361** (1978), 245.
13. R. B. HEYWOOD, "Design against Fatigue" (Chapman and Hall, London, 1962).
14. D. E. PUTTICK and A. G. ATKINS, *Int. J. Fract.* **23** (1983) R51.
15. P. LUDWIK, "Elemente der tech. Mech." (Berlin, 1909).
16. E. OROWAN, *Rep. Prog. Phys.* **12** (1949) 214.
17. *Idem, ibid.* **12** (1949) 1855.
18. C. GURNEY and J. HUNT, *Proc. R. Soc.* **A299** (1967) 508.
19. A. G. ATKINS and Y. W. MAI, "Elastic and Plastic Fracture: Metals, Polymers, Ceramics, Composites, Biological Materials" (Horwood/Wiley, Chichester, 1985).
20. Y. W. MAI and A. G. ATKINS, *Int. J. Mech. Sci.* **20** (1978) 437.
21. K. PUTTICK, *Proc. ICM-3* **3** (1979) 11.
22. A. A. GRIFFITH, *Phil. Trans. R. Soc.* **A221** (1921) 163.
23. *Idem*, Proceedings 1st International Congress on Applied Mechanics, Delft (1924).
24. G. R. IRWIN, in Proceedings of the Symposium on Effects of Temperature on Brittle Behaviour (American Society for Testing and Materials, Philadelphia, 1954) p. 176.
25. T. E. STANTON and R. G. C. BATSON, *Proc. Inst. Civil Eng.* **211** (1921) 67.
26. J. G. DOCHERTY, *Engineering* **139** (1935) 211.
27. *Idem, ibid.* **133** (1932) 645.
28. P. E. SHEARIN, A. E. RUARK and R. M. TRIMBLE, in "Fracturing of Metals" (ASM, Cleveland, 1948) p. 167.
29. K. HAGIAWARA, H. TAKANABE and H. KAWANO, *Int. J. Impact Eng.* **1** (1983) 257.

30. V. KUMAR, W. W. WILDENING, W. R. ANDREWS, M. D. GERMAN, H. G. de LORENZI and D. F. MOWBRAY, EPRI/GE Report SRD-82-048 (1982).
31. F. M. BURDEKIN, *Proc. Inst. Mech. Eng.* **195** (1981) 73.
32. H. J. FROST and M. F. ASHBY, "Deformation Mechanism Maps" (Pergamon, Oxford, 1982).
33. J. F. KNOTT, "Fundamentals of Fracture Mechanics" (Butterworths, London, 1973).
34. K. E. PUTTICK, *J. Phys. D Appl. Phys.* **11** (1978) 595.
35. P. KENNY and J. D. CAMPBELL, *Prog. Mater. Sci.* **13** (1968) 135.
36. J. C. JAEGER and N. G. W. COOK, "Fundamentals of Rock Mechanics" (Chapman and Hall, London, 1976).
37. A. G. ATKINS, *Int. J. Prod. Res.* **12** (1974) 263.
38. *Idem*, Proceedings NAMRC-II, Madison, Wisconsin, 1974 (Society of Automotive Engineers, Dearborn, Michigan) p. 398.
39. British Standard 5782 (1979)
40. A. G. ATKINS and Y. W. MAI, *Int. J. Fract.* **27** (1985) R103.
41. E. H. ANDREWS, *J. Mater. Sci.* **9** (1974). 887.
42. J. R. RICE, in "Fracture", Vol. 2, edited by H. Leibowitz (Academic Press, New York, 1968) p. 191.
43. C. RUIZ and R. S. J. CORRAN, *Int. J. Press. Ves. Piping* **10** (1982) 361.
44. W. SOETE, Proceedings ICF-4 Waterloo, Canada, Vol. I (Pergamon, Oxford, 1977).
45. C. RUIZ, *Int. J. Mech. Sci.* **20** (1976) 277.
46. R. S. J. CORRAN, P. H. DAVIES and C. RUIZ, *Eng. Fract. Mech.* **16** (1982) 585.
47. A. R. DOWLING and C. H. A. TOWNLEY, *Int. J. Press. Ves. Piping* **3** (1975) 77.
48. R. A. SMITH, in "Fracture and Fatigue" 3rd European Colloquium on Fracture, London, edited by J. C. Randon (1980) p 49.
49. R. M. RIVETT, *Welding Inst. Res. Bull.* **20** (1979) 235.
50. J. R. GRIFFITHS and G. OATES, Proceedings ICF-2, paper 19 (1969).
51. K. E. PUTTICK, L. S. A. SMITH and L. E. MILLER, *J. Phys. D Appl. Phys.* **10** (1977), 617.

*Received 16 July*
*and accepted 16 September 1985*